Nucleation Mechanism and Morphology of Polystyrene/Fe_3O_4 Latex Particles via Miniemulsion Polymerization Using AIBN as Initiator

Ying-Da Luo,[1] Chi-An Dai,[1,2] Wen-Yen Chiu[1,2,3]

[1]*Institute of Polymer Science and Engineering, National Taiwan University, Taipei, Taiwan, Republic of China*
[2]*Department of Chemical Engineering, National Taiwan University, Taipei, Taiwan, Republic of China*
[3]*Department of Material Science and Engineering, National Taiwan University, Taipei, Taiwan, Republic of China*

Received 23 March 2008; accepted 10 October 2008
DOI 10.1002/app.29481
Published online 23 January 2009 in Wiley InterScience (www.interscience.wiley.com).

ABSTRACT: In this study, oil-based magnetic Fe_3O_4 nanoparticles were first synthesized by a coprecipitation method followed by a surface modification using lauric acid. Polystyrene/Fe_3O_4 composite particles were then prepared via miniemulsion polymerization method using styrene as monomer, 2,2′-azobisisobutyronitrile (AIBN) as initiator, sodium dodecyl sulfate (SDS) as surfactant, hexadecane (HD) or sorbitan monolaurate (Span20®) as costabilizer in the presence of Fe_3O_4 nanoparticles. The effects of Fe_3O_4 content, costabilizer, homogenization energy during ultrasonication, and surfactant concentration on the polymerization kinetics (e.g., conversion), nucleation mechanism, and morphology (e.g., size distributions of droplets and latex) of composite particles were investigated. The results showed that at high homogenization energy, an optimum amount of SDS and hydrophobic costabilizer was needed to obtain composite particles nucleated predominately by droplet nucleation mechanism. The morphology of the composite particles can be well controlled by the homogenization energy and the hydrophobicity of the costabilizer. The magnetic composite particles can be made by locating Fe_3O_4 inside the latex particles or forming a shell layer on their PS core surface depending on the aforementioned polymerization conditions. © 2009 Wiley Periodicals, Inc. J Appl Polym Sci 112: 975–984, 2009

Key words: miniemulsion polymerization; magnetic composite particles; particle nucleation; morphology

INTRODUCTION

In the past few years, synthesis of magnetic polymer composite particles has drawn increasingly more attention because of their vast applications in cell separation,[1,2] enzyme immobilization,[3] environment and food analysis,[4] magnetic resonance imaging,[5] and targeting drug delivery.[6,7] The growing popularity of using such functional composite particles in biotechnology and medical diagnostics was because of their superb sensitivity in response to the external applied magnetic field and easy separation by magnetic separation.

Many different polymerization methods have been developed to prepare composite polymer colloids containing magnetic particles including the conventional emulsion polymerization,[8,9] precipitation polymerization,[10] suspension polymerization,[11] seeded polymerization,[12,13] soapless emulsion polymerization,[14] miniemulsion polymerization,[15–20] and so on.[21–24] In the method of miniemulsion polymerization to synthesize colloids containing magnetic particles, the magnetic particles were first undergone a surface modification using organic acids, in which the carboxyl functional group can anchor on the surface of iron particles.[25] The surface modified magnetic particles were subsequently dispersed in monomer, and the monomer droplets containing magnetic particles can act as nanoreactors for polymerization *in situ*. Lu and Forcada[17] examined the effects of the experimental parameter on the encapsulation degree of magnetic PS composite particles, such as surfactant concentration, hydrophobe concentration, stabilizer, and comonomer concentration. Ramirez and Landfester[18] synthesized magnetic polystyrene particles with high magnetite content successfully and developed a novel three-step miniemulsion preparation route. Lin et al.[19] produced thermoresponsive magnetic composite particles, with Fe_3O_4 homogeneously distributed in NIPAAm, via W/O miniemulsion polymerization.

Miniemulsion polymerization was widely taken as an effective method to prepare polymer/inorganic composite particles. In addition to Fe_3O_4, there were other types of inorganic particles being studied. Erdem et al.[26] produced TiO_2/PS composite particles

Correspondence to: W.-Y. Chiu (ycchiu@ccms.ntu.edu.tw).
Contract grant sponsor: National Science Council of Taiwan, Republic of China; contract grant number: NSC-95-2221-E-002-152.

and described the encapsulation efficiency using hydrophilic or hydrophobic TiO_2 particles in the presence of OLOA370® as stabilizer. Peres et al.[27] produced green-emitting CdSe/poly(butyl acrylate) nanocomposite particles and investigated the morphology and electrical property. In addition, carbon black/PS,[28] ZnO/PS,[29] and $CaCO_3$/PS[30] composite particles were also obtained by miniemulsion polymerization. However, regardless to what polymerization methods or inorganic material were used, most of the research in literature emphasized only the preparation and characterization of miniemulsion polymerization. There were few papers discussing the control of morphology and nucleation mechanism in polymer/inorganic composite particles.

The aim of this article was to examine how polymerization conditions affected the morphology of PS/Fe_3O_4 composite particles, the nucleation mechanism, and the polymerization kinetics through the course of miniemulsion polymerization.

EXPERIMENTAL

Materials

Styrene was distilled under a reduced pressure and was stored at 5°C before use. Hexadecane (HD; Acros), 2,2′-azobisisobutyronitrile (AIBN; Showa), sodium dodecyl sulfate (SDS; Acros), lauric acid (Acros), sorbitan monolaurate (Span20®; Showa) and 28% ammonium hydroxide solution (Acros) were used without further purification. Distilled and deionized water was used throughout the work.

Preparation of oil-based Fe_3O_4 particles

Fe_3O_4 particles were obtained by coprecipitation of Fe(II) and Fe(III) salts in aqueous solution of ammonium hydroxide. In this process, 23.5 g $FeCl_3 \cdot 6H_2O$ and 8.6 g $FeCl_2 \cdot 4H_2O$ were dissolved in 400 mL deionized water with stirring. Then 50 mL of 28% (w/w) ammonium hydroxide solution was added in the mixed iron chloride solution for 6 min. Additional 2.5 g lauric acid was added to the solution under stirring at 90°C for 30 min to modify the surfaces of Fe_3O_4 particles to become hydrophobic in nature. Finally, the supernatant solution was decanted, and the surface modified Fe_3O_4 black residue was washed with methanol for three times to remove any nonbonded lauric acid. Then, the precipitates were lyophilized for 24 h to obtain the oil-based Fe_3O_4 particles.

Preparation of PS/Fe_3O_4 composite particles by miniemulsion polymerization

In a typical miniemulsion experiment, two types of solution were prepared prior to the miniemulsification, for example, aqueous-phase and oil-phase solutions. The aqueous phase solution was composed of deionized water and SDS, and the oil phase solution was composed of styrene, Fe_3O_4, HD, and AIBN. The synthesis recipe for this study is shown in Table I in detail. Both solutions were each stirred for 10 min before mixing by mechanical stirring. After mixing, the oil-in-water mixture was ultrasonicated in an ice bath using a Hielscher UP-50H ultrasonicator. Ice bath was used to prevent polymerization during ultrasonication. The ultrasonication time and amplitude were the two parameters to be discussed in this study. Finally, the homogenized miniemulsion solution was poured into a 250 mL four-necked glass reactor equipped with a condenser and a mechanical stirrer in a water bath. The stirring rate was kept at

TABLE I
Symbols and Recipes for Synthesized Composite Particles[a]

	Fe_3O_4 (%)	SDS (m*M*)	Costabilizer	Energy	AIBN (wt %)
F0	0	35	HD	50%, 13 min	2.5
F1	10	35	HD	50%, 13 min	2.5
F2	20	35	HD	50%, 13 min	2.5
E1	10	35	HD	50%, 13 min	2.5
E2	10	35	HD	50%, 30 min	2.5
E3	10	35	HD	100%, 30 min	2.5
S1	10	20	HD	100%, 30 min	2.5
S2	10	35	HD	100%, 30 min	2.5
S3	10	70	HD	100%, 30 min	2.5
H1	10	35	HD	50%, 13 min	2.5
P1	10	35	Span 20	50%, 13 min	2.5
H2	10	35	HD	100%, 30 min	2.5
P2	10	35	Span 20	100%, 30 min	2.5

[a] Styrene + Fe_3O_4 = 13.89 g, Costabilizer concentration = 51 m*M*. The percentage of initiator was based on monomer.
The percentage of Fe_3O_4 was based on styrene + Fe_3O_4.
The concentration of surfactant or costabilizer was based on water.

300 rpm, and the polymerization was carried out for 1.5 h at 85°C.

Conversion

The conversion of monomer after polymerization was determined by a gravimetric method. During the miniemulsion polymerization, a certain amount of the latex was taken out of the reactor and poured into a hydroquinone methanol solution in an ice bath. Finally, the sample was dried in an oven at 85°C until the sample weight was constant. The polymerization conversion could be calculated by eq. (1) where P is the dried sample weight, F is the theoretical weight of Fe_3O_4 in the sample, W is the weight of the latex sample, and M_0 is the weight fraction of monomer in the feed recipe.

$$\text{Conversion} = \frac{P - F}{W \times M_0} \times 100\% \quad (1)$$

Morphology of oil-based Fe_3O_4 and PS/Fe_3O_4 composite particles

The PS/Fe_3O_4 composite latex particles were diluted with deionized water, and the oil-based Fe_3O_4 particles were dispersed in toluene. The solution was then dropped on cooper grids and dried for TEM measurement. The morphology and size of the magnetic particles were measured by using a JOEL JEM-1230 transmission electron microscope.

Size distributions of monomer droplets and composite latex particles

The size distributions of the monomer droplets and the resulting composite latex particles were measured by a dynamic light scattering instrument (Malvern Zeta Sizer 3000H). The sample was diluted in H_2O with saturated concentration of styrene (3.65 m*M*) and critical micelle concentration of SDS (8.2 m*M*) to avoid monomer or SDS diffusing from droplets to aqueous solution. The measurements were completed within several minutes, and the size distribution was obtained and plotted by taking particle diameter as the horizontal axis, the instantaneous or cumulative volume percentage as the vertical axis.

Magnetization curve of oil-based Fe_3O_4 and composite latex particles

The magnetization curves of the composite latex particles and oil-based Fe_3O_4 nanoparticles were measured with a Quantum Design MPMS5 superconducting quantum interference device (SQUID) magnetometer at 298 K with a ± 10,000-G applied magnetic field. The measurement examined the superparamagnetic properties of the Fe_3O_4 that was incorporated into the composite latex particles. In addition, the saturated value of magnetization, remanence, and coercivity were also determined.

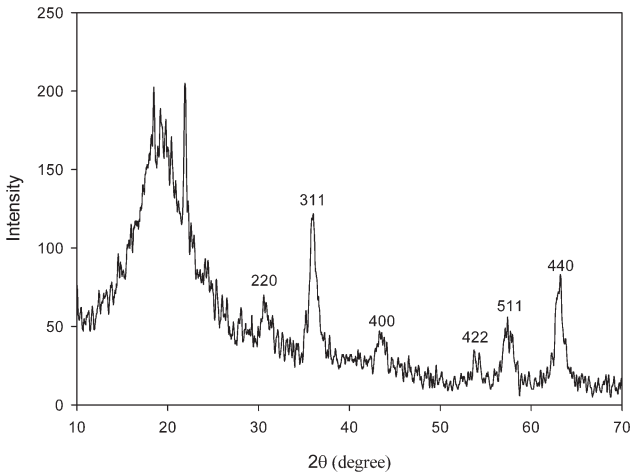

Figure 1 XRD pattern of the oil-based Fe_3O_4 nanoparticles.

RESULTS AND DISCUSSION

Oil-based Fe_3O_4 particles

Figure 1 shows the XRD pattern of the surface modified oil-based Fe_3O_4 particles. The characteristic peaks for the particles were identical to those of pure unmodified Fe_3O_4 particles with crystalline structure of spinel phase.[31] However, the peaks were broader because of some noncrystalline portions of the Fe_3O_4 particles. The mean diameter of the particles was calculated from the XRD pattern by the Debye-Scherrer equation as shown in eq. (2),[32,33] in which D is the average diameter of the Fe_3O_4 crystal, λ is the wavelength of the X-ray (Cu Kα = 1.54 Å), β is the width of the characteristic peak at half height, and θ is the diffraction angle. The values of β and θ from crystalline plane (3 1 1) were used in eq. (2). The size of the surface modified Fe_3O_4 crystal was calculated to be around 7.1 nm.

$$D = \frac{0.9\lambda}{\beta \cos\theta} \quad (2)$$

The value of D was close to the diameter observed from TEM micrograph shown in Figure 2. The particle diameter of the magnetic Fe_3O_4 nanoparticles shown in the TEM micrograph ranged from 6 to 9 nm.

PS/Fe_3O_4 composite particles

Effect of the content of Fe_3O_4

The conversion curves of the resulting composite latex particles with different amount of Fe_3O_4 were shown in Figure 3. With increasing amount of the

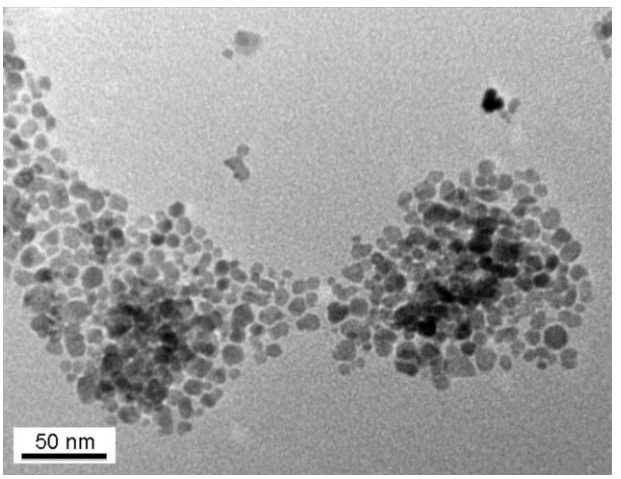

Figure 2 TEM photograph of the oil-based Fe_3O_4 nanoparticles.

Fe_3O_4, the polymerization rate and the final conversion decreased. The decrease in rates and conversion was because of an increase in the concentration of free radical quencher, Fe^{3+} ion, from the presence of Fe_3O_4 to inhibit the polymerization.[24] As a result, when more Fe_3O_4 was added in the polymerization solution, the polymerization was less effective, and the polymerization rate and the final conversion decreased. Figure 4 shows the size distributions of the initial monomer droplets and final latex particles with different Fe_3O_4 contents in both cumulative and its differential forms. The sample F2 (with 20% Fe_3O_4), showed broad droplet size distribution, and the diameter ranged from 300 to 600 nm. For the sample F1 (with 10% Fe_3O_4), its droplet size distribution shifted to smaller values, in a range between 200 and 500 nm. For the Fe_3O_4 free sample (F0), 50% of the droplets had diameter less than 200 nm.

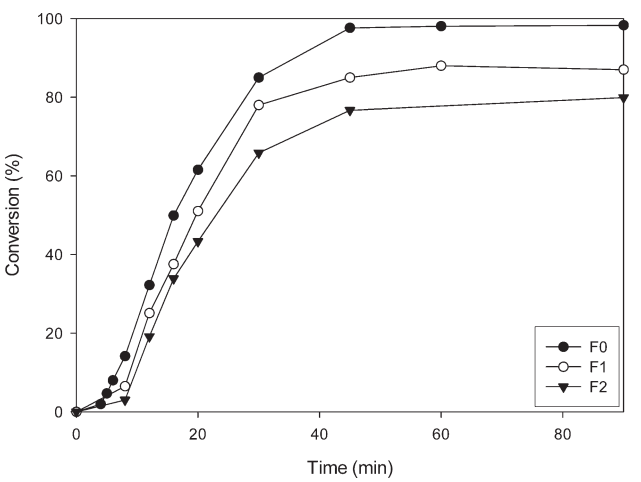

Figure 3 Monomer conversion versus time with different amount of Fe_3O_4. The formulation was shown in Table I.

When the monomer was miniemulsified to droplets, the size distribution of droplets was determined by both ultrasonication energy and Ostwald ripening. Ultrasonication induced droplet fission, and Ostwald ripening resulted in monomer transportation from small droplets to large droplets. Initially, the size distribution of droplets was unimodal and shifted to smaller values under ultrasonication. However, the Ostwald ripening became more significant due to the difference of size in droplets. It resulted in the bimodal size distribution of droplets during the process of ultrasonication. With further ultrasonication, the monomer would be totally emulsified to the droplets with critically stabilized sizes. To this point, the emulsion is stable, and the size distribution of droplets is unimodal again. In the formulation of F0, F1, and F2 in Figure 4, the ultrasonication amplitude and duration time were all set as 50% and 13 min. Under such experimental condition, the homogenization energy was too low to obtain an emulsion with critically stabilized size of

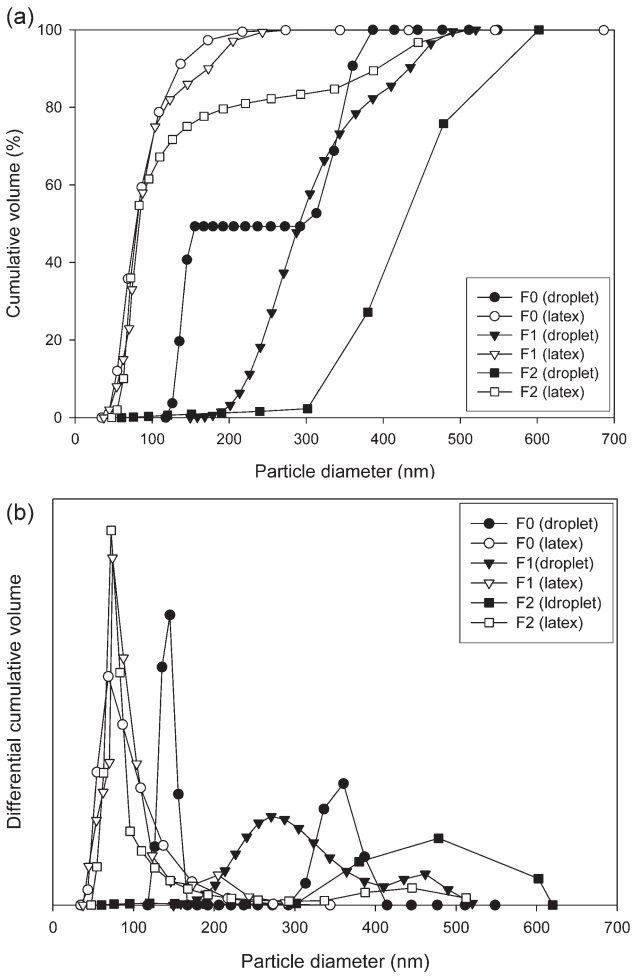

Figure 4 Size distributions of droplets and latex particles with different amount of Fe_3O_4.(a) cumulative form (b) differential form.

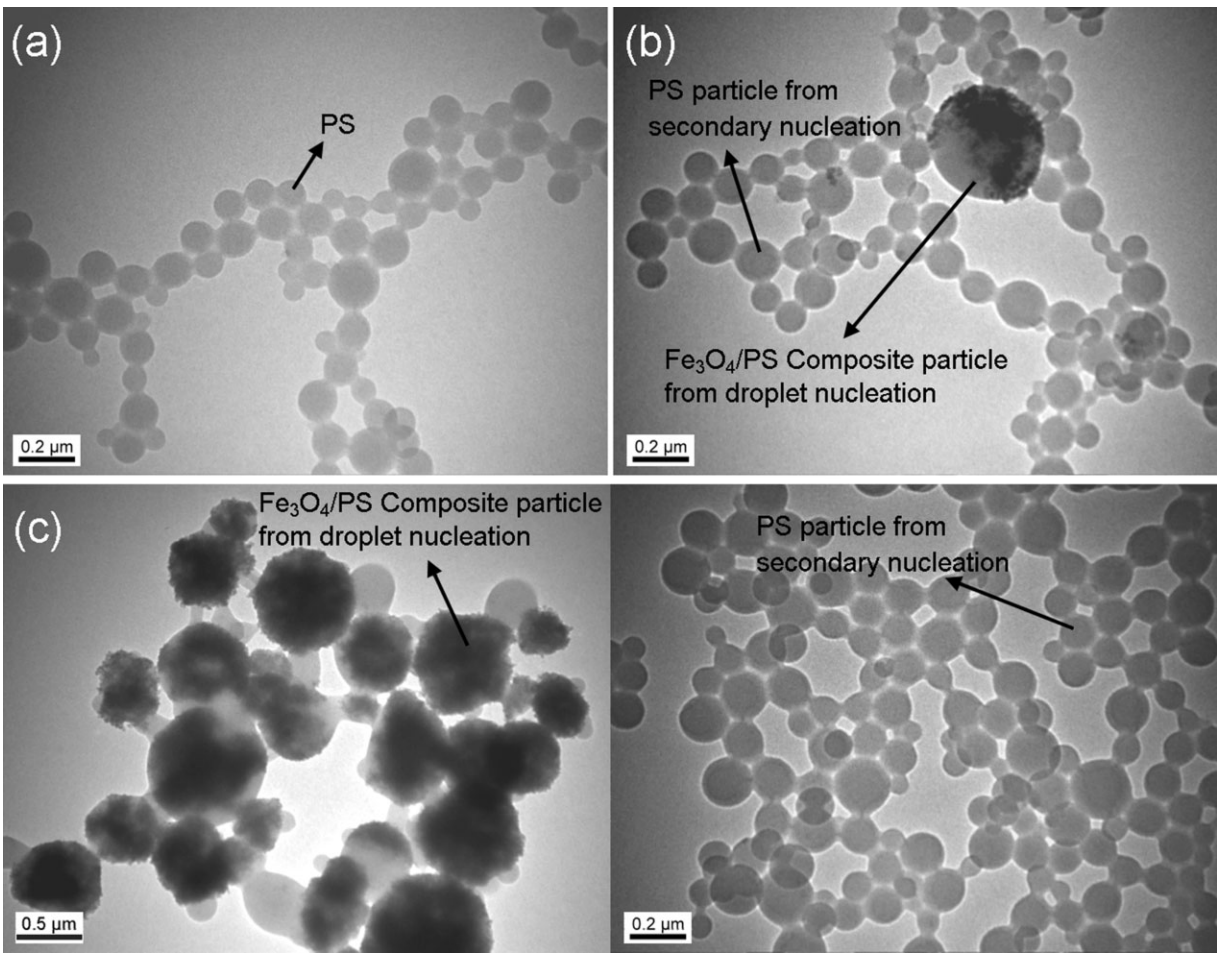

Figure 5 TEM photographs of synthesized composite latex particles with different amount of Fe_3O_4. The formulation was shown in Table I. (a) F0, (b) F1, E1, H1, and (c) F2.

droplets. In sample F2, the higher content of Fe_3O_4 reduced the efficiency of droplet fission during ultrasonication so that the bimodal size distribution was not yet observed. In Fe_3O_4 free sample, F0, the size distribution of droplets was bimodal. It indicated that the droplet fission was more efficient under the same ultrasonication condition. As for sample F1, the size distribution lay between F0 and F2.

After polymerization, sample F1 and F2 both had bimodal particle size distribution. The part of larger size particles mainly formed from the shrinking of original droplets, and the part of smaller size particles mainly came from the secondary nucleation. For the sample F0, a unimodal particle size distribution was obtained because a comparable amount of particles originated from droplet shrinking, and the secondary nucleation mechanism resulted in a continuous size distribution. Nevertheless, from the comparison of droplet and latex particle size distributions in these three experimental conditions, a large population of composite particles formed from the mechanism of secondary nucleation.

TEM photographs of the obtained composite particles were shown in Figure 5. The TEM results were consistent with the particle size distribution obtained from the dynamic light scattering experiment. Two kinds of particles were observed, Fe_3O_4/PS composite particles and pure PS particles. The composite particles, larger in size, were from droplet nucleation. The pure PS particles, smaller in size, were from secondary nucleation. With a higher content of Fe_3O_4, the size of larger composite particles increased. The reason was that larger original droplets resulted in larger composite particles even after shrinking.

Effect of the homogenization energy

The homogenization energy applied to the O/W emulsion could be varied by adjusting the ultrasonication time and amplitude. The longer ultrasonication time and higher ultrasonication amplitude presented higher input energy. In Figure 6, the conversion curves of the composite latex showed that

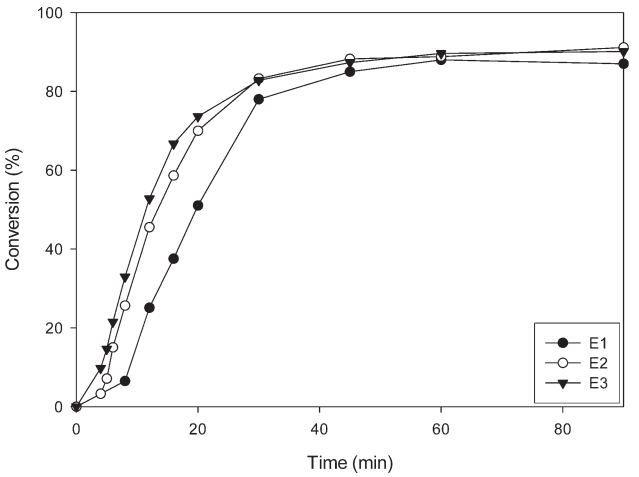

Figure 6 Monomer conversion versus time with different homogenization energy. The formulation was shown in Table I.

with increasing ultrasonication energy, the polymerization rate increased. It appeared that as more energy was applied to the O/W emulsion, larger droplets tended to be broken into smaller droplets. In other words, during polymerization, the reaction sites for droplet nucleation increased and the polymerization rate was enhanced.

This explanation was further verified from the results of the size distributions of droplets and particles with different homogenized energy as shown in Figure 7. As the total homogenization energy increased, the sample E3 (100% ultrasonic amplitude for 30 min) showed much smaller average diameter and narrower size distribution for both droplets and particles than that of E1 (50% ultrasonic amplitude for 13 min) with less ultrasonic amplitude and duration time. Furthermore, the sample E3 showed similar size distributions between the droplets before polymerization and the composite particles after polymerization. The result indicated that the secondary nucleation mechanism was largely reduced. In other words, most particles were formed from the droplet nucleation mechanism. However, for both the samples E1 and E2, there was a significant feature of size shrinkage after polymerization, which might be because of the fact that a critically stabilized size of droplets has not yet been achieved before polymerization. Therefore, the secondary nucleation was more dominant over the droplet nucleation especially for the sample of E1. It could be concluded that the homogenization energy played an important role to control the nucleation mechanism, and suitable homogenization energy was required to attain droplet nucleation.

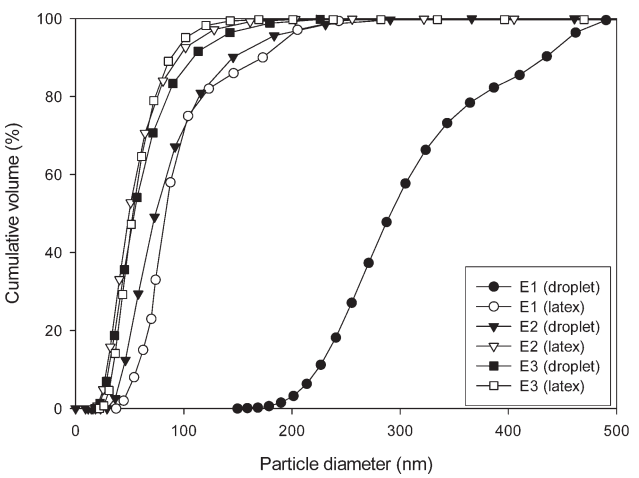

Figure 7 Size distributions of droplets and latex particles with different homogenization energy. The formulation was shown in Table I.

TEM photographs of the synthesized composite particles were shown in Figure 5(b) for sample E1 and in Figure 8 for sample E3, respectively. These micrographs showed that the morphology of Fe_3O_4/PS composite particles was significantly changed from a relatively uniform dispersion of Fe_3O_4 within PS particle to a core-shell structure with Fe_3O_4 on the shell layer. The change in the morphology may be resulted from the fact that with increasing homogenization energy during ultrasonication, Fe_3O_4 particles were forced to migrate out onto the droplets surface due to the large density difference between Fe_3O_4 and styrene monomer.

Effect of surfactant concentration

The surfactant, SDS, was added in the polymerization solution to prevent droplets from coalescence and to provide enough electrostatic repulsion to maintain the stability of monomer droplets. The conversion curves with different surfactant

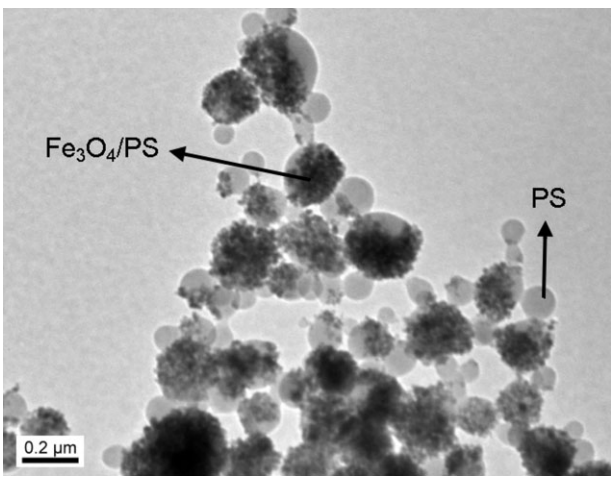

Figure 8 TEM photograph of synthesized composite particles E3, S2, and H2.

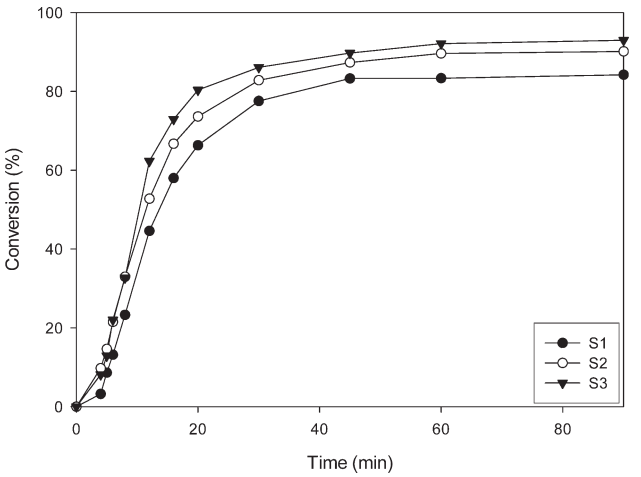

Figure 9 Monomer conversion versus time with different amount of SDS. The formulation was shown in Table I.

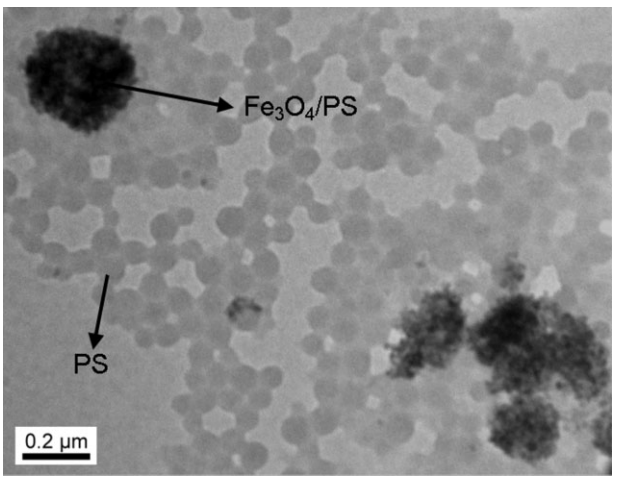

Figure 11 TEM photograph of synthesized composite particles S1.

concentrations were shown in Figure 9. Figure 9 shows that the polymerization rate increases with increasing surfactant concentration in the order of S1 (20 m*M* of SDS), S2 (35 m*M*), and S3 (70 m*M*). It could be explained by Figure 10, in which the average size of the monomer droplets was in the order of S3 < S2 < S1. As the amount of surfactant increased, more surfactants were able to stabilize the oil and water interface. Monomers could be broken into smaller droplets during the process of ultrasonication. Because small monomer droplets acted as reaction loci, the polymerization rate was increased with increasing the number of droplets and the average size of composite particles decreased.

After polymerization, the size shrinking phenomenon of the resulting particles comparing to the size of their initial droplets was more pronounced in S1 and S3 than in S2 as the average diameter of composite particles was smaller than that of their corresponding initial droplets. This above results indicated that S2 had an optimum surfactant concentration among the three for miniemulsion polymerization. For S1, the surfactant was insufficient in amount to provide enough stabilization for O/W interface, thus resulted in an enhanced possibility of secondary nucleation. As for S3, there were superfluous surfactants in solution to form micelles. Monomer could diffuse from droplets into micelles and induced micellar nucleation. In our study, an optimum surfactant concentration of 35 m*M* for SDS was found to achieve droplet nucleation. For the sample S2, the size distributions of the droplets and composite particles were similar, indicating that droplet nucleation mechanism dominated.

Furthermore, by comparing the TEM photographs of S1 and S2 (shown in Fig. 11 and Fig. 8, respectively), large amount of pure PS latex particles were observed for S1 due to the increase of secondary nucleation mentioned above.

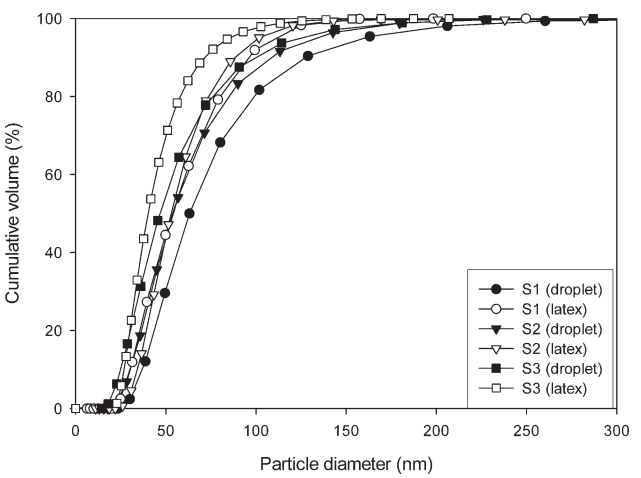

Figure 10 Size distributions of droplets and latex particles with different amount of SDS. The formulation was shown in Table I.

Effect of the costabilizer

The role of adding costabilizer in miniemulsion formulation was to suppress Oswald ripening effect by introducing an osmotic pressure to maintain droplet stability during polymerization. In this series of experiment, HD and Span20® were chosen as two different types of costabilizer. Although HD is a highly hydrophobic compound, Span20® is a relatively more hydrophilic one due to its shorter hydrocarbon chain and three hydrophilic hydroxyl functional groups. Their structures were shown in Scheme 1. Because of the amphiphilic nature of Span20®, it could also be used as a surfactant (HLB = 8.6). The conversion curves for miniemulsion of H1 (HD and ultrasonic amplitude 50% for 13 min),

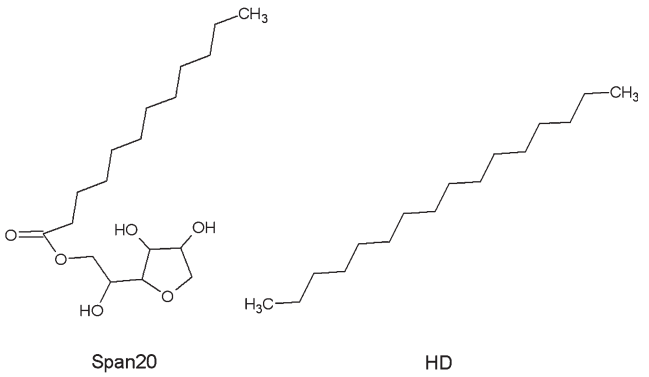

Scheme 1 Chemical structure of the costabilizer.

P1 (Span20® and ultronsonic amplitude 50% for 13 min) and H2 (HD and ultrasonic amplitude 100% for 30 min), P2 (Span20® and ultronsonic amplitude 100% for 30 min) were shown in Figure 12. Regardless, the homogenization energy was high or low, when the costabilizer changed from HD to Span20®, the polymerization rate was accelerated. It was because that Span20® acted not only as a costabilizer but also as a surfactant such that more surfactant was available to stabilize the O/W interface during ultrasonication. Thus more monomer droplets could act as the reaction site. The result could be verified by the size distribution curves of H2 and P2 as in Figure 13. The size of droplet of P2 was smaller than that of H2 as expected.

By comparing the size distributions of droplets and latex particles for H2 and P2, it could be found that sample H2 had 50% of monomer droplets with the same size distribution as latex particles, while only 30% for H2. The result showed that hydrophobic costabilizer, HD, increased the possibility of droplet nucleation.

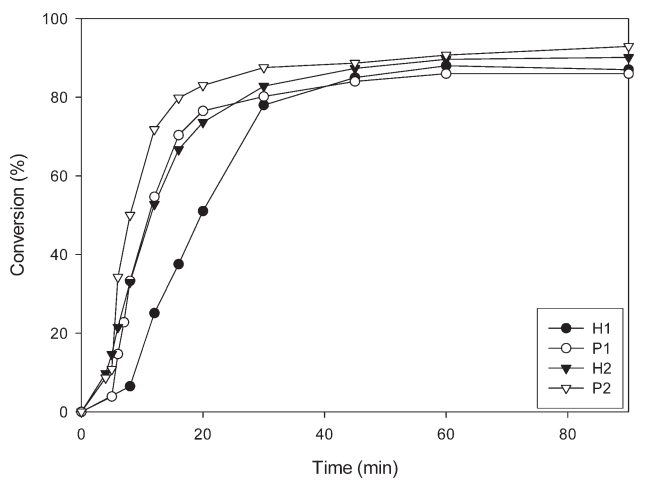

Figure 12 Monomer conversion versus time with different costabilizer. The formulation was shown in Table I.

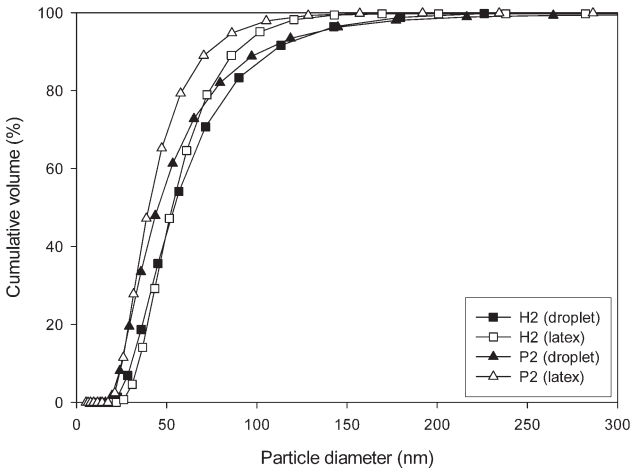

Figure 13 Size distributions of droplets and latex particles with different costabilizer. The formulation was shown in Table I.

The morphology difference with different costabilizer was observed by the TEM measurement shown in Figure 5(b) and Figure 14(a). The morphology of composite particles changed from homogeneous latex particles for H1 to a core-shell structure with Fe_3O_4 on the shell layer for P1. This was resulted from the more hydrophilic structure of Span20®, which brought Fe_3O_4 particles out onto the surfaces from the monomer droplets during ultrasonication or during the early stage of polymerization, whereas Fe_3O_4 particles still distributed homogeneously in styrene droplets when using HD as a costabilizer. The morphology of H2 and P2 [shown in Fig. 8 and Fig. 14(b), respectively] was all in a core-shell structure. A homogeneous morphology was not observed when high homogenization energy was applied.

Magnetization curve of composite latex particles

Finally, the superparamagnetic properties of the oil-based Fe_3O_4 nanoparticles and composite latex particles, sample E3, were examined. Their magnetization curves were shown in Figure 15. The saturated value of magnetization of oil-based Fe_3O_4 particles was about 60 emu/g of iron oxide. The amount of iron oxide in the oil-based Fe_3O_4 nanoparticles was about 87%, determined from TGA measurement (data not shown here). Furthermore, the remanence and coercivity were zero, and no magnetic hysteresis loop was observed in Figure 15. These results revealed that the Fe_3O_4 nanoparticles synthesized were superparamagnetic. For the magnetic composite latex particles, the original SQUID data showed that the saturated value of magnetization of composite latex particles was about 4.5 emu/g of composite latex particles. The TGA measurement revealed only 7 wt % in the composite latex particles was iron

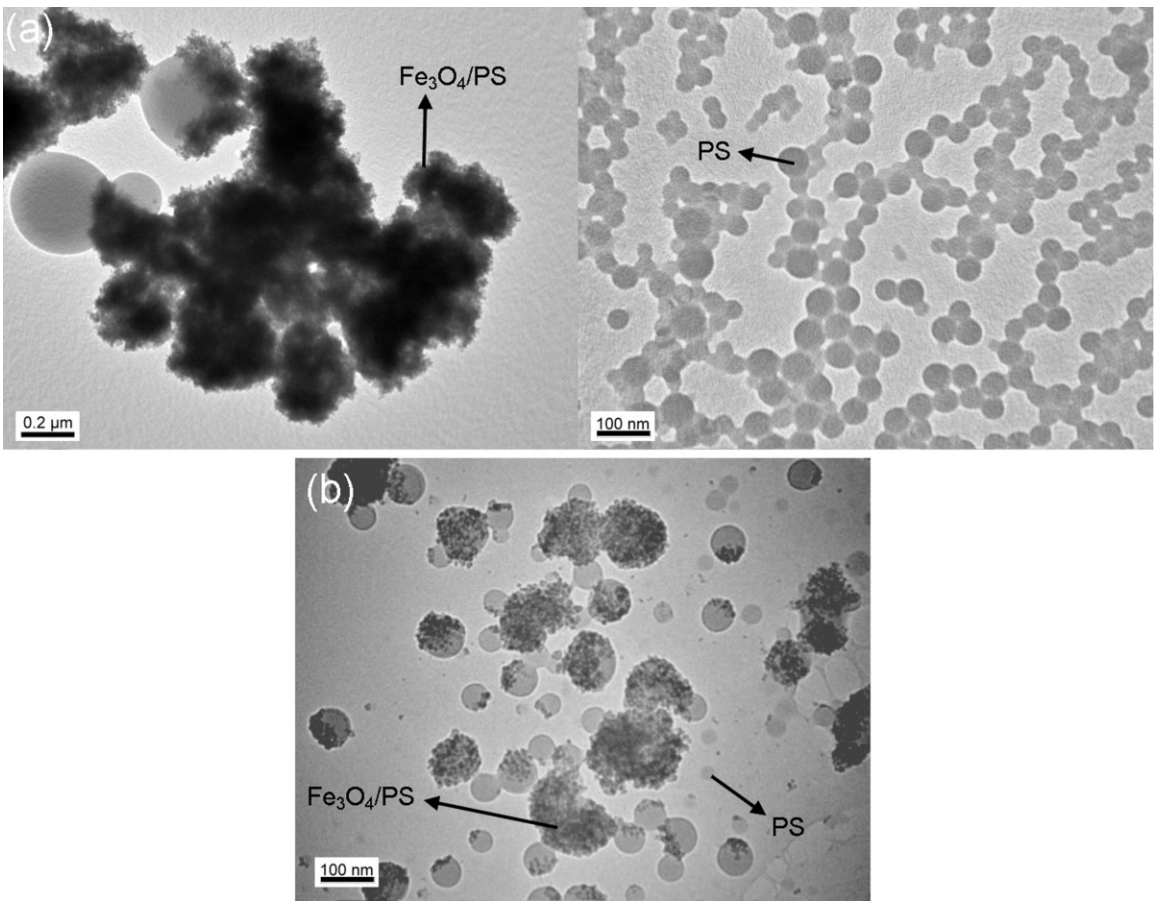

Figure 14 TEM photographs of synthesized composite particles. (a) P1 and (b) P2.

oxide (data not shown). When the magnetization curve of composite latex particles was normalized to emu/g of iron oxide in Figure 15, the saturated value of magnetization was also about 60 emu/g. It could be concluded that the intrinsic properties of the magnetic nanoparticles were not changed after the polymerization process.

CONCLUSIONS

In this work, PS/Fe_3O_4 composite particles were successfully synthesized using a miniemulsion polymerization method. The conversion, size distributions of monomer droplets and the resulting magnetic composite latex particles, the nucleation mechanism, and the particle morphology were discussed in detail. The polymerization rate was significantly promoted by increasing the number of monomer droplets, which was achieved under the condition of high concentration of surfactant, higher homogenization energy or changing costabilizer from HD to Span20®. Because of the role of Fe^{3+} from Fe_3O_4 acting as a free radical quencher, higher content of Fe_3O_4 in the reaction system would reduce the polymerization rate.

The size distributions of droplets and latex particles were measured and compared to estimate the fraction of droplet nucleation. With increasing the Fe_3O_4 content, the size distribution of droplets and latex particles were broader with more population of larger particles due to the less efficiency of droplet

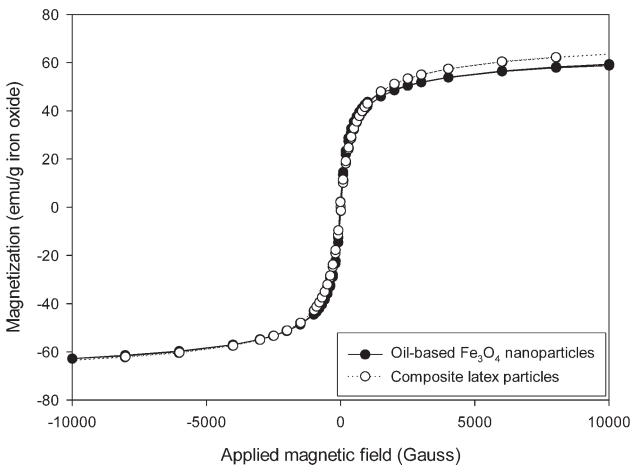

Figure 15 Magnetization curve of oil-based Fe_3O_4 nanoparticles and magnetic composite latex particles.

fission during ultrasonication. For high homogenization energy, the monomer droplets were critically stabilized such that the size distributions of monomer droplets and the resulting latex particles were almost identical. The function of SDS was to provide stabilization for oil/water interface and an optimum concentration was found. Too much surfactant resulted in micelle formation and micellar nucleation. However, insufficient amount of surfactant could not maintain the stability of monomer droplets and secondary nucleation could not be avoided. The choice of costabilizer was critical too, more hydrophobic one, HD, was effective to produce osmotic pressure and to resist Oswald ripening effect. Thus, the stability of monomer droplets was enhanced and polymerization *in situ*, droplet nucleation dominated.

The morphology of the composite latex particles could be controlled by changing both the homogenization energy and the type of costabilizer used. For high homogenization energy, the Fe_3O_4 located on the surface of PS latex particles. It differed from the one with low homogenization energy, in which Fe_3O_4 was randomly and quite uniformly distributed inside the latex particles. When HD was used as a costabilizer, a random and quite homogeneous morphology was observed for composite particles only if the homogenization energy was not high. However, the core–shell morphology with Fe_3O_4 on the shell of composite particles was observed if Span20® replaced HD as a costabilizer. The more hydrophilic nature of Span20® changed the location of Fe_3O_4 particles and induced the morphology change. The morphology control could afford different applications of these magnetic composite particles.

References

1. Haik, Y.; Pai, V.; Chen, C. J. J Magn Magn Mater 1999, 194, 254.
2. Sieben, S.; Bergemann, C.; Lubbe, A.; Brockmann, B.; Rescheleit, D. J Magn Magn Mater 2001, 225, 175.
3. Akgol, S.; Kacar, Y.; Denizli, A.; Arica, M. Y. Food Chem 2001, 74, 281.
4. Pyle, B. H.; Broadaway, S. C.; McFeters, G. A. Appl Environ Microbiol 1966 1999, 65.
5. Cheng, F. Y.; Su, C. H.; Yang, Y. S.; Yeh, C. S.; Tsai, C. Y.; Wu, C. L.; Wu, M. T.; Shieh, D. B. Biomaterials 2005, 26, 729.
6. Viroonchatapan, E.; Ueno, M.; Sato, H.; Adachi, I.; Nagai, H.; Tazawa, K.; Horikoshi, I. Pharm Res 1995, 12, 1176.
7. Gupta, P. K.; Hung, C. T. Life Sci 1989, 44, 175.
8. Yanase, N.; Noguchi, H.; Asakura, H.; Suzuta, T. J Appl Polym Sci 1993, 50, 765.
9. Horak, D.; Petrovsky, E.; Kapicka, A.; Frederichs, T. J Magn Magn Mater 2007, 311, 500.
10. Deng, Y. H.; Yang, W. L.; Wang, C. C.; Fu, S. K. Adv Mater 2003, 15, 1729.
11. Pollert, E.; Knizek, K.; Marysko, M.; Zaveta, K.; Lancok, A.; Bohacek, J.; Horak, D.; Babic, M. J Magn Magn Mater 2006, 306, 241.
12. Wang, P. C.; Chiu, W. Y.; Lee, C. F.; Young, T. H. J Polym Sci Polym Chem 2004, 42, 5695.
13. Montagne, F.; Mondain-Monval, O.; Pichot, C.; Elaissari, A. J Polym Sci Polym Chem 2006, 44, 2642.
14. Pich, A.; Bhattacharya, S.; Adler, H. J. P. Polymer 2005, 46, 1077.
15. Csetneki, I.; Faix, M. K.; Szilagyi, A.; Kovacs, A. L.; Nemeth, Z.; Zrinyi, M. J Polym Sci Polym Chem 2004, 42, 4802.
16. Wormuth, K. J Colloid Interface Sci 2001, 241, 366.
17. Lu, S. H.; Forcada, J. J Polym Sci Polym Chem 2006, 44, 4187.
18. Ramirez, L. P.; Landfester, K. Macromol Chem Phys 2003, 204, 22.
19. Lin, C. L.; Chiu, W. Y.; Don, T. M. J Appl Polym Sci 2006, 100, 3987.
20. Luo, Y. D.; Dai, C. A.; Chiu, W. Y. J Polym Sci Polym Chem 2008, 46, 1014.
21. Deng, Y.; Wang, L.; Yang, W.; Fu, S.; Elaissari, A. J Magn Magn Mater 2003, 257, 69.
22. Ma, Z. Y.; Guan, Y. P.; Liu, H. Z. J Polym Sci Polym Chem 2005, 43, 3433.
23. Lee, C. F.; Chou, Y. H.; Chiu, W. Y. J Polym Sci Polym Chem 2007, 45, 3912.
24. Lee, C. F.; Chou, Y. H.; Chiu, W. Y. J Polym Sci Polym Chem 2007, 45, 3062.
25. Kataby, G.; Cojocaru, M.; Prozorov, R.; Gedanken, A. Langmuir 1999, 15, 1703.
26. Erdem, B.; Sudol, E. D.; Dimonie, V. L.; El-Aasser, M. S. Macromol Symp 2000, 155, 181.
27. Peres, M.; Costa, L. C.; Neves, A.; Soares, M. J.; Monteiro, T; Esteves, A. C.; Barros-Timmons, A.; Trindade, T.; Kholkin, A.; Alves, E. Nanotechnology 1969, 2005, 16.
28. Tiarks, F.; Landfester, K.; Anonietti, M. Macromol Chem Phys 2001, 202, 51.
29. Zhang, J. J.; Gao, G.; Zhang, M.; Zhang, D.; Wang, C. L.; Zhao, D. C.; Liu, F. Q. J Colloid Interface Sci 2006, 301, 78.
30. Bechthold, N.; Tiarks, F.; Willert, M.; Landfester, K.; Antonietti, M. Macromol Symp 2000, 151, 549.
31. Schwertmann, U.; Cornell, M. R. Iron Oxides in the Laboratory, Preparation and Characterization; VCH: New York, 1991.
32. Taylor, A. X-Ray Metallography; Wiley: New York, 1961.
33. Massart, R.; Cabuil, V. J Chim Phys-Chim Biol 1987, 84, 967.